16. Majumdar, K., *Curr. Sci.*, 2004, **86**, 1288–1292.
17. Beroza, G. C. and Ellsworth, W. L., *Tectonophysics*, 1996, **261**, 209–227.
18. Madden, T. and Mackie, R., *Proc. Natl. Acad. Sci. USA*, 1996, **93**, 3776–3780.
19. Fraser-Smith, A. C., Bernardi, A., McGill, P. R., Ladd, M. E., Helliwell, R. A and Villard, O. G., *Geophys. Res. Lett.*, 1990, **17**, 1465–1468.
20. Galper, A. M., Koldashov, S. V., Murashov, A. M., Ozerov, Y. V. and Voronov, S. A., www.pereplet.ru/pops/quakes/quakes.html, 1995, pp. 1–5.
21. Rikitake, T., Oshiman, N. and Hayashi, M., In *Developments of Solid Earth Geophys.*, Elsevier, 1976, no. 9.
22. Hatai, S. and Abe, N., *Proc. Imp. Acad. Jpn.*, 1932, **8**, 375–378.
23. Suyehiro, Y., *Bull. Earthquake Res. Inst. Univ. Tokyo, Suppl.*, 1934, **1**, 228–231.
24. Tereda, T., *Bull. Earthquake Res. Inst. Univ. Tokyo*, 1931, **10**, 393–401.
25. Skinner, B. J. and Porter, S. C., In *The Dynamic Earth, An Introduction to Physical Geology*, John Wiley, 2000, 4th edn, p. 396.
26. Beresnev, I. A. and Johnson, P. A., *Geophysics*, 1994, **59**, 1000–1017.
27. Wakita, H., Igarshi, G., Nakamura, Y., Sano, Y. and Notsu, K., *Geophys. Res. Lett.*, 1989, **16**, 417–420.
28. Abercrombie, R. E. and Mori, J., *Nature*, 1966, **381**, 303–307.

ACKNOWLEDGEMENTS. We are grateful to the Department of Science and Technology, New Delhi and the Department of Atomic Energy, Government of India, for sponsoring the present activities.

Received 11 January 2005; revised accepted 23 June 2005

Relocation of earthquakes in the Northeast Indian region using joint hypocentre determination method

Pankaj Mala Bhattacharya[1,*], Jose Pujol[2], R. K. Majumdar[3] and J. R. Kayal[1]

[1]Central Geophysics Division, Geological Survey of India, 27, J. L. Nehru Road, Kolkata 700 016, India
[2]Centre for Earthquake Research and Information, The University of Memphis, Memphis, TN 38152, USA
[3]Department of Geological Sciences, Jadavpur University, Kolkata 700 032, India

A set of 1941 earthquake events recorded in the northeast region of India during January 1993 – December 1999 was used for relocation by the Joint Hypocentre Determination (JHD) technique. We have utilized both *P*- and *S*-wave arrivals recorded by closely spaced 77 temporary and permanent seismic stations in the region. Results of this analysis show that (a) the average root mean square travel time residual becomes smaller than the corresponding single event locations by the HYPO71; (b) station correction varies from –2.43 to 2.32 s for *P*-wave, and from –2.84 to 2.84 s for *S*-wave, indicating large crustal velocity variations in the region; (c) positive station corrections are obtained in the Shillong Plateau, Assam valley and in the Manipur fold belt, and negative station corrections are obtained in the Mikir hills, and (d) lateral variation of the velocity structure inferred from station corrections is comparable with that obtained by 3D velocity inversion using the local earthquake tomography method.

Keywords: Earthquake, joint hypocentre determination, lateral velocity variation, local earthquake tomography, station correction.

THE tectonic characteristics of the northeast region of India, lat. 24–28°N and long. 89–98°E, are complicated and unique in many aspects (Figure 1). Over the last few decades, a number of investigations on seismicity and tectonics of this region have been carried out[1–4]. These authors mostly used HYPO71 to locate earthquakes recorded by temporary seismic stations. Kayal and Zhao[5] made an attempt to relocate the earthquakes by 3D inversion using temporary network data in the Shillong Plateau, southwest part of the region (Figure 1). Bhattacharya *et al.*[6] did fractal dimension and *b*-value studies in this region. Precise earthquake locations play an important role in understanding earthquake source processes. The earth's crust and upper mantle consist of heterogeneous structures on a regional scale. This includes complications such as discontinuities, faults, layering and random geological heterogeneities. Such complicated three-dimensional velocity structures affect the quality of locations. The effect of heterogeneous crustal velocity structure in earthquake location can be minimized by use of the Joint Hypocentre Determination (JHD) technique, which has the capability of producing significantly improved relative locations[7–9]. The technique owes its success to the fact that the JHD station corrections partially compensate for the lateral velocity variations, thus improving the relative location of the hypocentres.

Many authors use the Average Residual Method (ARM) for locating earthquakes[10,11]. The average residual is taken as station correction to minimize the travel time residual, but if the velocity model used to compute theoretical travel times is incorrect, minimization of the residual does not assure well-located events[9]. Therefore, using the average of the individual station residuals will not necessarily improve locations. The JHD method is designed to minimize all travel-time residuals simultaneously and to find a common set of station corrections. The events are, however, not free to move to locations that they would have when located individually. This loss of freedom results in an increase of the station residuals, which are absorbed in the station correction terms[12].

In this study, an attempt has been made to use the JHD method to relocate earthquakes and to obtain *P*- and *S*-wave station corrections in the Northeast Indian region. Both *P*- and *S*-wave first-arrival observations recorded during the

*For correspondence. (e-mail: gsicgd@cal2.vsnl.net.in)

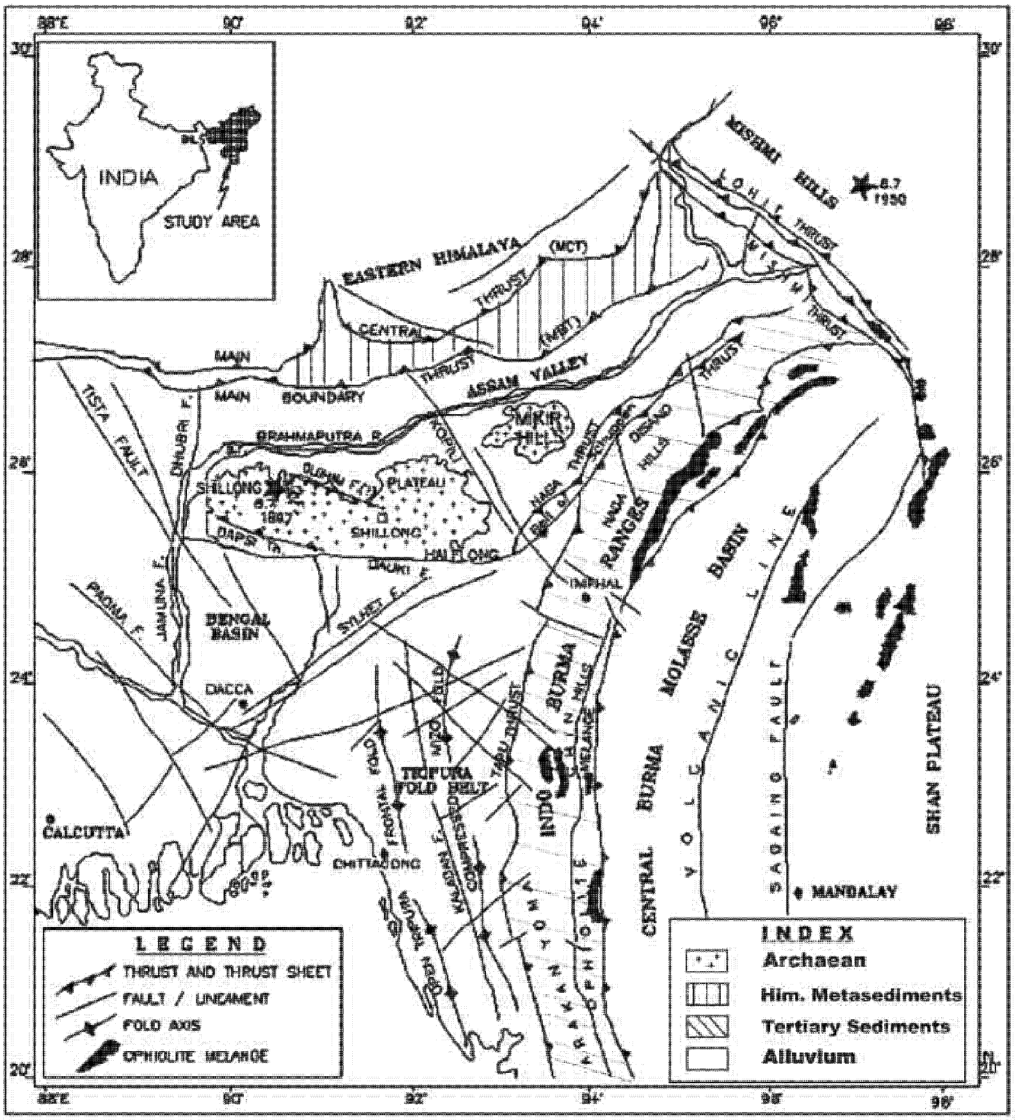

Figure 1. Map showing major tectonic features and epicentres (solid circles) of large earthquakes ($M \geq 7.0$) in the region (Kayal[32]). Two great earthquakes ($M > 8.0$) are shown (star symbols). MCT, Main Central Thrust; MBT, Main Boundary Thrust; DF, Dauki Fault; DT, Dapsi Thrust; KL, Kopili Lineament. Major geological formations are also shown. Black patches in the Indo-Burma ranges indicate ophiolites. (Inset) Key map of study area.

period January 1993 – December 1999 by 77 permanent and temporary seismograph stations are used. The improved locations of the events and the station corrections are studied in terms of seismicity and crustal heterogeneties of the region. The crustal heterogeneities thus obtained are compared with the 3D inversion of the velocity structure at shallow depth by the Local Earthquake Tomography (LET) method[13].

Northeast India and adjoining areas fall in the most intense seismic zone, i.e. zone V in the seismic zoning map of India (Figure 1). Two great earthquakes ($M > 8.0$), the 1897 great Shillong earthquake (M_S 8.7), and the 1950 great Assam earthquake (M_L 8.7), and 18 large earthquakes occurred in this region[4]. The region is in juxtaposition to the east-west Himalayan collision zone to the north and the north-south Indo-Burma subduction zone to the east (Figure 1). Earthquakes in the Himalayan arc are shallow and referred to collision tectonics, and the seismicity is correlated with the known regional thrusts, the Main Boundary Thrust (MBT) and the Main Central Thrust (MCT)[14] (Figure 1). Earthquakes in the Arunachal Himalaya, however, are reported to occur down to a depth of 80 km[15]. Although mostly thrust faulting is reported for the teleseismic earthquakes in the Himalayan arc[16], microearthquake investigation revealed transverse seismogenic structure beneath the Arunachal Himalaya[15,17]. Earthquakes in the Burmese arc, on the other hand, are referred to subduction tectonics; normal, thrust and strike-

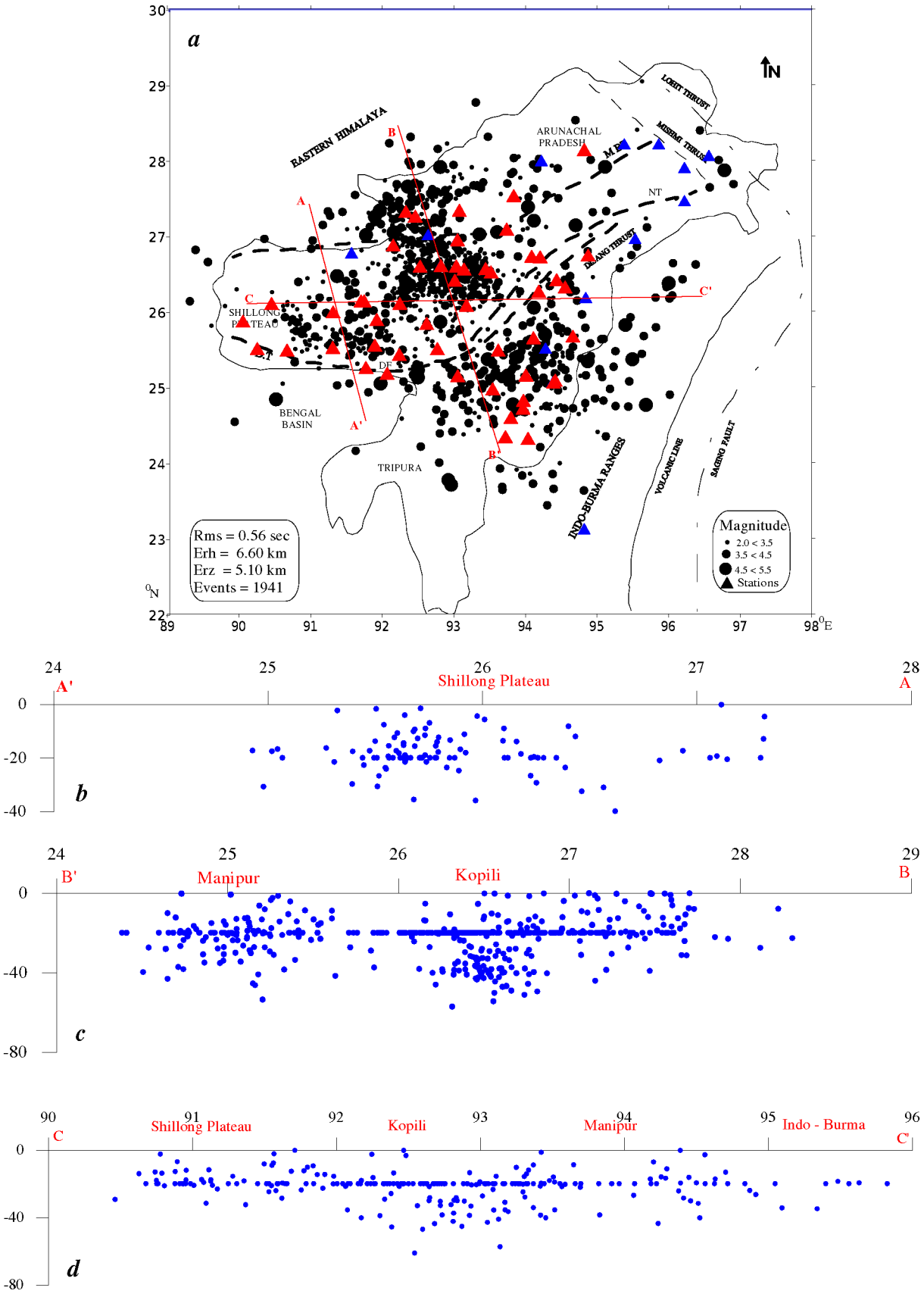

Figure 2. (*a*) Map showing station locations and epicentres of selected 1941 events located by HYPO71. Stations used in final JHD locations are shown in red triangles. Cross-sections are shown along AA′ (*b*), BB′ (*c*) and along CC′ (*d*).

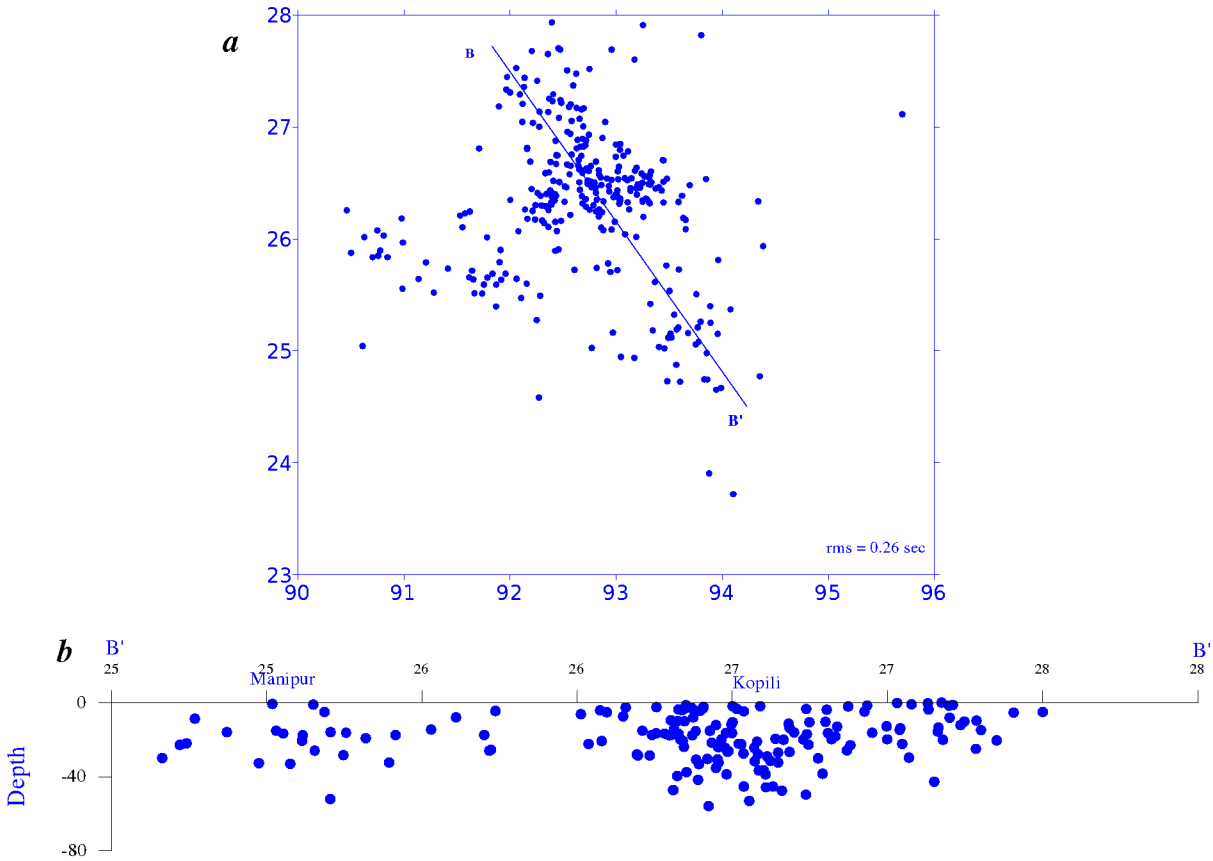

Figure 3. Epicentres of 316 events relocated by JHD (*a*) and cross-section along BB′ (*b*).

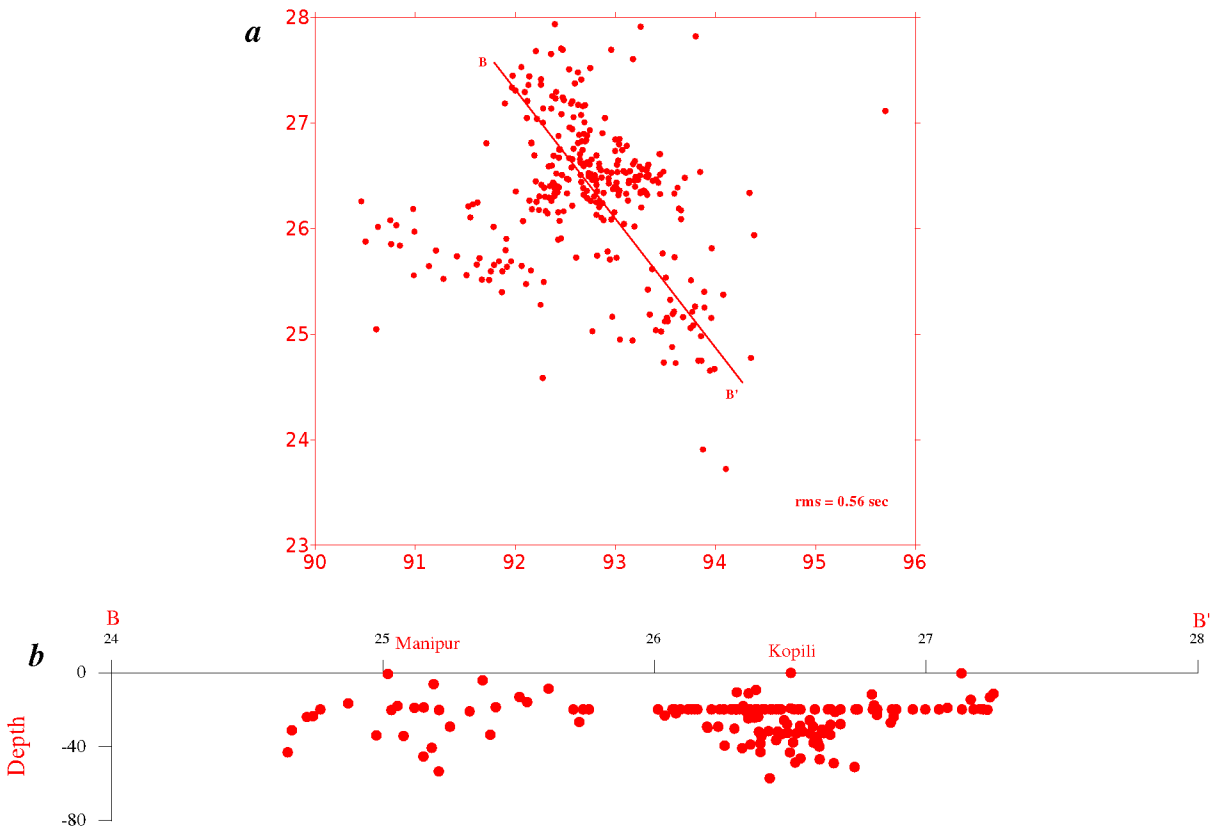

Figure 4. Epicentres of 316 events located by Hypo71 (*a*), and cross-section along BB′ (*b*).

Table 1. One-dimensional velocity model (after De and Kayal[24])

V_P (km/s)	Depth (km)
5.55	0
6.52	20
8.10	41
8.57	46

Table 2. One-dimensional velocity model estimated by LET method

V_P (km/s)	Depth (km)
5.56	0
6.10	10
6.45	20
6.90	30
7.60	40
8.40	50

slip faulting are reported[4,18–20]; earthquakes are as deep as 200 km in the subducted Indian plate. The meeting zone of the Himalayan arc and the Burmese arc, the eastern syntaxis zone in the Mishmi hills, is also seismically active and was the source area of the 1950 great Assam–Tibet earthquake (M_L 8.7). The Shillong Plateau and Assam valley area, bounded by the MBT to the north and by the Dauki fault to the south, is well known for its high seismic activity and has been the seat of the 1897 great Shillong earthquake (M_S 8.7). Earthquakes in the Shillong Plateau region are mostly confined within a depth ranges 20–35 km; reverse faulting and strike-slip faulting are reported[2,3]. To the east of the Shillong Plateau lies the Mikir massif, which is separated from the Shillong massif by a NW–SE major lineament/fault called the Kopili lineament[21]. The Mikir hills area is equally active as the Shillong Plateau area[3].

The northeast region of India is well instrumented with digital and analogue microearthquake networks. Permanent and temporary seismic stations have been established since 1980 by the Geological Survey of India (GSI), National Geophysical Research Institute (NGRI), Hyderabad, Regional Research Laboratory, Jorhat (RRL-J), and by several local universities. The permanent network data are published in the form of seismological bulletins by the NGRI and RRL-J. Station locations are shown in Figure 2. Coordinated Universal Time (UTC) is maintained by radio signal for the analogue stations and by GPS clock for digital stations. The overall timing accuracy of ± 0.1 s is maintained for the analogue telemetric stations (NGRI and RRL-J bulletins). Time accuracy for *P*-arrivals recorded by the temporary stations were read with a precision of ± 0.05 s and overall accuracy[2,3] was maintained ± 0.1 s. The S-wave arrivals were, however, read with ± 0.5 s precision. The three-component digital seismograms provided high-precision *P*-wave (± 0.01 s) and *S*-wave (± 0.05 s) arrival times.

A total of 3190 events were used in this study, which were recorded during the period 1993–99 in this region. The *P*- and *S*-arrival times were assigned weights depending upon the confidence of time-picking, particularly for the analogue records. The unreliable *S*-phase data were removed by plotting Wadati diagrams[22]. The scatter *S*-phase data showing larger fluctuations from the least square fit line were discarded. Several V_P/V_S ratios (1.70–1.78) have been tried. We found that the V_P/V_S ratio of 1.72 was the most suitable initial value for our dataset. The *P*- and *S*-arrival data were used to make preliminary estimates of the hypocentral parameters using HYPO71 program[23].

A homogenous 1D velocity model (Table 1)[24] and a constant V_P/V_S of 1.72 were used for preliminary locations of the 3190 events by HYPO71. Events that could not be located with root mean square (rms) travel-time residuals lesser than 1.0 s were eliminated. This preliminary screening led to a selection of 1941 events with an average rms of 0.68 s. In the next stage we used the LET method of Thurber[13], modified by Eberhart-Phillips[25], for estimating the average 1D velocity structure of the area using the 1941 selected events. We then incorporated the estimated 1D model (Table 2) to relocate the events using HYPO71 and found that the average rms reduced from 0.68 to 0.56 s. Epicentres of the events and a few cross-sections are shown in Figure 2. The epicentre map indicates fairly well the azimuthal coverage of the seismic stations, almost all the events are located with AZM (azimuth gap) < 180°.

In order to ensure that JHD relocation would provide reliable results, only events that satisfied certain criteria were selected. The selection criteria were: (i) Well-recorded events with magnitude greater than or equal to 2.5; (ii) rms error less than 1.0 s, and (iii) number of *P*- and *S*-phases for an event no less than 4 and 2 respectively. An integer weight factor between 0 and 4 was assigned to each observation depending on the quality of the reading. The JHD algorithim used in the present study was introduced by Pavilis and Booker[26] and later modified by Pujol[8].

The JHD method simultaneously solves for station corrections and hypocentral parameters. Station corrections can be viewed as representing deviations of the actual velocity structure from the layered assumed model used in the joint location. The positive and negative corrections generally correspond to low- and high-velocity anomalies respectively[27]. JHD inversion is iterative, and convergence is achieved in a few iterations (usually five or less). Station correction in a few seismic stations could not be evaluated. These stations are rejected by the JHD technique and are marked using blue colour in Figure 2.

Several quantities determined during JHD computations are useful to establish the quality of the results. Singular values of the matrix that is inverted at each iteration to determine the station corrections, are of particular importance. One of the singular values is equal to zero, which reflects nonuniqueness of the solution due to trade-off between origin time and station corrections. If none of the remaining

singular values is zero, then JHD locations can be uniquely determined. Further, the ratio of the largest to the smallest nonzero singular value gives an indication of the numerical stability of the results. Another indicator of numerical stability is the sum of the station corrections, which should be equal to the sum of the initial estimates respectively[27]. The *S*-wave station corrections are calculated as if there were two separate stations (for *P* and for *S*) for each physical location of a seismic station. The *S*-wave station corrections are calculated separately, but not independently of the *P*-wave corrections, because *S*-wave travel times are obtained using a fixed V_P/V_S ratio.

JHD computations were carried out with the inverted 1D velocity model (Table 2). A layered 1D velocity model is obviously too simple to describe the complexity of the real earth. No matter how many layers the crustal model incorporates, large travel-time residuals will occur at the stations where the earth's crust does not conform to the crustal model. One way to compensate for the inaccuracy of the crustal model is to apply station corrections, which constrain event locations better.

Only the events recorded by at least four stations having quality weights of 0 or 1 (0: best; 4: worst) were selected. This reduced the number of events to 1044. Thus out of 1941 events, only a subset of 1044 events were used for relocation. We calculated the event parameters as well as station corrections, which consequently require the use of inversion.

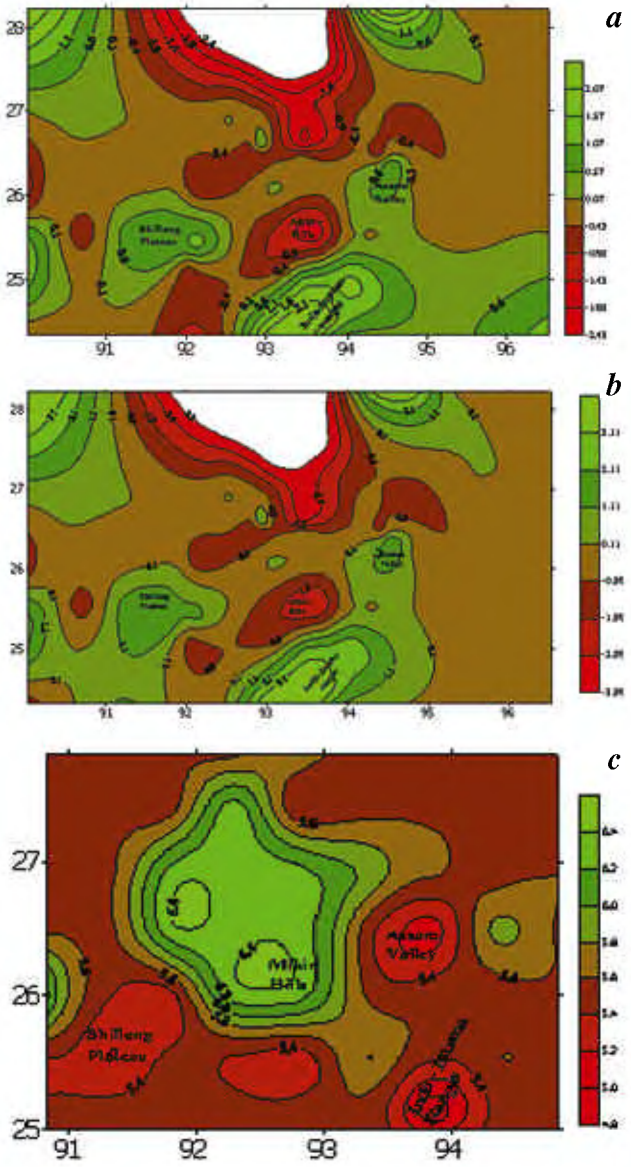

Figure 5. Contour map of (*a*) *P*-wave station correction and (*b*) *S*-wave station correction (station correction in seconds). (*c*) *P*-wave velocity image at a depth of 5 km using LET.

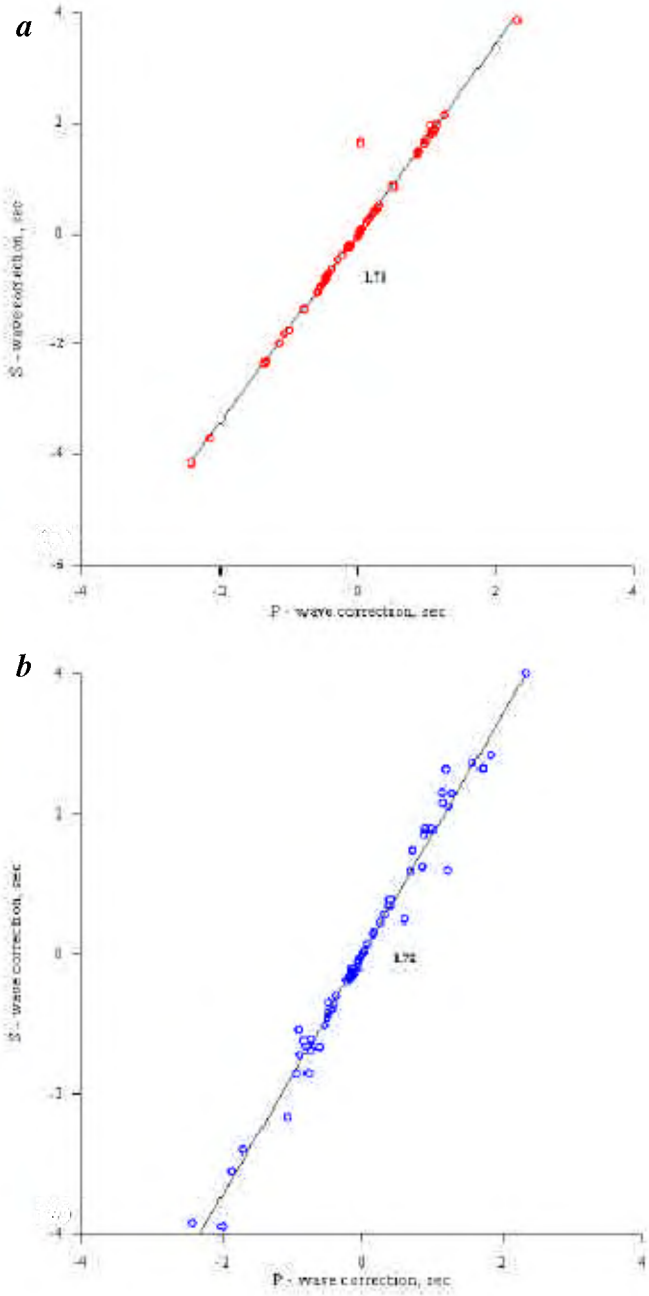

Figure 6. *S*-wave station correction versus *P*-wave station correction for (*a*) observed data and (*b*) synthetic data.

For the first iteration, we choose a set of station corrections. For subsequent iterations, events were relocated by applying station corrections. The iterations were stopped when the station corrections converged and minimum rms error of travel-time residuals was obtained. During JHD computations, the cut-off rms residual was 0.3 s in the last iteration. Although all the selected 1044 events were used in JHD computations, the number of events were reduced to 316 after five iterations. There was a large rejection on the basis of the JHD criteria. This was probably because of some analogue data in which the timing precision of the data was not as good as the digital data, and we had no scope to recheck the analogue seismograms. The rejected events had individual rms residuals larger than a cut-off value of 0.3 s. Thus, 316 events are relocated by the JHD method. The epicentres are shown in Figure 3 *a*. A cross-section of the clustered events is shown in Figure 3 *b*. For comparison, these 316 events are again located by HYPO71 using 1D velocity model (Table 2); the epicentres along with a cross-section are shown in Figure 4. Station corrections computed by JHD for *P*- and *S*-waves are illustrated in Figure 5 *a* and *b*.

A 3D velocity model was determined using the LET technique[13,25]. This 3D velocity model was then used to generate synthetic arrival times using JHD technique. Synthetic data are treated exactly the same way as the observed data. Results of analysis of the synthetic data are used as an independent check of the results obtained from the analysis of observed data. A comparison of the station corrections obtained by the observed and synthetic data for both *P*- and *S*-waves is shown in Table 3. It may be noted that the JHD station corrections determined from the synthetic data are close to those obtained from the observed data. The average difference between the corresponding corrections is 0.04 s for *P*-wave and 0.05 s for *S*-wave.

Since station corrections are mostly dependent on the lateral heterogeneity of the velocity structure at shallow depth, the *P*-wave velocity structure at a shallower depth (depth < 5 km) is estimated using LET method as mentioned above. For choosing the area for 3D velocity study, we examined the seismograph station locations, initial HYPO71 estimates of epicentres and maximum depth extent of the events (Figure 2). We set up grid nodes with a grid spacing 50 km in horizontal plane and 10 km in vertical plane. The spatial distribution of the epicentres was considered to fix the spread of the model along east-west and north-south directions. Along both the directions the model was restricted within 250 km, keeping the centre of the model at 26°N and 93°E. The estimated velocity image at a depth of 5 km is illustrated in Figure 4 *c*. A detailed study of deeper seismic structure (10 to ~ 40 km) is given by Bhattacharya *et al.*[28].

Seismicity pattern of the northeast Indian region is critically studied by JHD method. The 1941 events were first located by HYPO71. Epicentres of the 1941 events, magnitude ≥ 2.5, and station locations are shown in Figure 2 *a*. The epicentre map shows three clusters of events; one in the Shillong Plateau, one in the Manipur Fold Belt and a most intense cluster along the Kopili lineament. On the basis of these clusters, three cross-sections of the events are examined, two NNW–SSE sections along AA′ and BB′, and one E–W section along CC′ respectively (Figure 2 *b–d*). Earthquakes that fall within 50 km on either side of the cross-section lines are considered. The section along AA′ across the Shillong Plateau shows that the activity below the Plateau is confined within a depth range of 15–35 km. The section BB′ illustrates two clusters of events, one below the Manipur Fold Belt and another below the Mikir hills/Arunachal Predesh along the Kopili fault. Earthquakes are deeper (30–40 km) below the Kopili fault compared to those below the Manipur Fold Belt (20–30 km). The E–W cross-section CC′ across the Shillong Plateau, Mikir hills and Indo-Burma ranges also depicts that the earthquakes are shallower in the Shillong Plateau (< 30 km) compared to that in the Mikir hills (30–40 km) or Kopili fault zone. In the Manipur Fold Belt, the earthquakes are also of shallow (< 30 km) origin. Not many earthquakes are, however, located in the Indo-Burma ranges, as the area falls much outside the network. Thus our study is mostly confined to the shallow crustal earthquakes in the study region. It may be noted that in the HYPO71 location program, foci of many events are fixed to the trial depth of 20 km (Figure 2 *b–d*).

Out of the 1941 selected events, only 316 events are relocated by the JHD method. The relocated epicentres are shown in Figure 3 *a* and the corresponding HYPO71 locations of these 316 events are shown in Figure 4 *a*. A visual examination shows that both the epicentre maps are comparable. Computational results, however, show that the average rms of 0.56 s obtained by the HYPO71 locations is reduced to 0.26 s by the JHD method. A relatively small value of rms does not always mean a corresponding small error in earthquake location, as the goal of the location programs is to minimize rms and not the location errors, which remain unknown as long as each earthquake is located separately[29]. The JHD technique, however, preserves the relative locations well, without introducing serious artifacts[29]. Improvement of earthquake relocations by the JHD method in depth direction is, in particular, significant. Figure 3 clearly depicts the improved depth estimates by the JHD method compared to those located at fixed (trial) depth (20 km) by the HYPO71 (Figure 4). This exemplifies the efficacy of the JHD method, which unfolded a true trend of the earthquakes at depths (Figure 3). The hypocentres are thus better located by the JHD method.

The parameters routinely used to monitor the quality of the JHD results are examined. The smallest singular value of the matrix inverted to compute the station corrections was equal to -0.08×10^{-4}, which is close to the expected value of zero. The smallest nonzero singular value and the largest one are equal to 0.02 and 19.02 respectively,

Table 3. JHD station corrections

Station code	Latitude °N	Longitude °E	*P*-wave			*S*-wave		
			Observed station correction	Synthetic station correction	Difference observed – synthetic	Observed station correction	Synthetic station correction	Difference observed – synthetic
ALN	28.15	94.79	1.57	1.06	0.52	2.73	1.97	0.77
BHD	26.28	94.15	0.6	0.32	0.29	0.5	0.53	–0.03
BHDI	26.28	94.15	0.03	0.02	0.02	0.05	0.02	0.04
BKD	26.89	92.12	–0.13	–0.51	0.38	–0.27	–0.88	0.61
BKG	26.09	93.14	0.16	0.01	0.16	0.29	–0.01	0.3
BMI	27.27	92.42	–0.89	–0.79	–0.11	–1.46	–1.36	–0.11
BPR	26.57	93.11	–0.4	–0.47	0.07	–0.73	–0.81	0.08
BOK	26.01	91.28	–0.07	–0.14	0.07	–0.18	–0.25	0.07
BOJ	26.76	94.84	–0.03	–0.1	0.07	–0.05	–0.18	0.13
BSP	24.61	93.76	2.32	2.31	0.02	4	3.87	0.14
CDL	24.33	94	0.91	0.04	0.88	1.79	1.65	0.15
CHK	26.43	94.4	–0.47	–0.47	0	–0.85	–0.8	–0.06
CHKI	26.43	94.4	–0.36	–0.27	–0.1	–0.61	–0.46	–0.16
CHA	24.32	93.99	0	–0.02	0.02	0	–0.04	0.04
CHP	24.35	93.68	1.13	1.07	0.06	2.31	1.78	0.54
CMD	25.5	93.58	–1.71	–1.15	–0.57	–2.8	–1.98	–0.83
CRP	25.27	91.74	0.88	0.87	0.02	1.71	1.48	0.24
DAG	26.79	91.54	0	0.06	–0.06	0	0.09	–0.09
DRG	27.33	92.29	–0.94	–0.5	–0.45	–1.71	–0.87	–0.85
DKI	25.19	92.03	–0.5	–0.48	–0.03	–0.9	–0.83	–0.08
DWK	25.19	92.03	0.69	0.51	0.19	1.17	0.86	0.32
DPJ	28.01	94.19	0	0.15	–0.15	0	0.25	–0.25
GAU	26.15	91.67	–0.18	–0.42	0.24	–0.35	–0.73	0.38
GOP	26.12	90.42	–0.06	–0.11	0.05	–0.1	–0.19	0.09
GWH	26.15	91.71	–0.05	–0.45	0.4	–0.09	–0.78	0.68
HYG	28.08	96.53	0	0.05	–0.05	0	0.07	–0.07
HLG	25.16	93.02	–0.76	–0.4	–0.37	–1.4	–0.7	–0.71
HLGA	25.16	93.02	0	–0.02	0.02	0	–0.04	0.04
HMN	25.85	92.58	1.18	1.06	0.13	2.63	1.82	0.82
HMNA	25.85	92.58	–0.13	–0.13	–0.01	–0.21	–0.23	0.02
IMP	24.84	93.94	1.82	1.15	0.68	2.84	1.98	0.87
INR	27.1	93.7	–1.07	–1.36	0.29	–2.32	–2.36	0.04
JHI	26.73	94.17	–0.19	–0.48	0.29	–0.33	–0.84	0.51
JWI	25.44	92.2	1.21	1.09	0.13	1.18	1.87	–0.69
JGR	26.12	92.21	–0.8	–0.21	–0.6	–1.33	–0.37	–0.97
KAZ	26.58	93.41	–1.87	–1.34	–0.54	–3.1	–2.32	–0.79
KHM	25.66	94.08	0.33	0.23	0.11	0.56	0.38	0.19
KHOU	24.73	93.93	1.27	0.97	0.31	2.3	1.64	0.67
KGN	26.76	94.84	0	0.05	–0.05	0	0.07	–0.07
KGNI	26.76	94.84	–0.62	–0.59	–0.04	–1.34	–1.01	–0.34
KOI	26.98	95.5	0	0.02	–0.02	0	0.02	–0.02
KZI	26.58	93.41	–0.84	–0.43	–0.42	–1.24	–0.74	–0.51
KPG	25.17	93.97	1.22	1.11	0.12	2.11	1.87	0.25
KDI	26.98	95.5	0	0.04	–0.04	0	0.06	–0.06
MAO	27.48	96.19	0	0.03	–0.03	0	0.04	–0.04
MKG	26.33	94.52	0.99	0.86	0.14	1.79	1.45	0.35
MLR	25.68	94.63	0.17	0.3	–0.13	0.32	0.49	–0.17
NGN	25.53	91.27	0.72	0.26	0.47	1.48	0.42	1.07
NGP	25.9	91.89	0.27	0.15	0.13	0.46	0.24	0.23
NGT	26.74	94.05	–0.75	–0.37	–0.39	–1.22	–0.63	–0.6
PBR	25.88	90.02	–0.9	–1.07	0.17	–1.09	–1.8	0.71
PNB	26.53	93.48	–0.48	–0.55	0.07	–0.7	–0.93	0.23
PNBI	26.53	93.48	–0.15	–0.13	–0.03	–0.29	–0.22	–0.08
PGT	28.23	95.35	0	0.13	–0.13	0	0.21	–0.21
ROG	28.23	95.83	0	0.27	–0.27	0	0.44	–0.44
SIL	26.61	93	0.4	0.23	0.18	0.78	0.38	0.41
SGR	26.61	92.49	–0.21	–0.61	0.4	–0.38	–1.05	0.67
SJA	26.96	93.01	–0.78	–0.48	–0.31	–1.7	–0.83	–0.88

(*Contd...*)

Table 3. (*Contd...*)

Station code	Latitude °N	Longitude °E	*P*-wave			*S*-wave		
			Observed station correction	Synthetic station correction	Difference observed – synthetic	Observed station correction	Synthetic station correction	Difference observed – synthetic
SNA	26.42	92.98	–0.54	–0.55	0.01	–1.02	–0.95	–0.08
SPA	27.35	93.04	–2	–2.42	0.42	–3.89	–4.14	0.25
SHL	25.57	91.86	0.86	0.89	–0.03	1.24	1.51	–0.27
TEZ	27.92	96.19	0	0.18	–0.18	0	0.29	–0.29
TML	24.99	93.51	1.14	1.01	0.14	2.16	1.71	0.46
TPI	27.03	92.61	0	0.06	–0.06	0	0.09	–0.09
TSG	26.2	94.81	0	0.06	–0.06	0	0.09	–0.09
TUR	25.52	90.22	0.39	0.15	0.25	0.69	0.25	0.45
TZR	26.62	92.78	–0.42	–1	0.58	–0.8	–1.74	0.94
UMI	25.52	92.73	0.08	0.13	–0.05	0.15	0.21	–0.06
UMS	25.52	92.73	–0.16	–0.41	0.25	–0.31	–0.71	0.4
UKH	25.08	94.35	–0.07	–0.12	0.05	–0.13	–0.21	0.08
UKL	25.1	94.38	1.71	1.25	0.47	2.64	2.15	0.5
WLN	25.5	90.63	–0.71	–0.4	–0.32	–1.33	–0.7	–0.64
WSL	25.53	94.25	0	0.01	–0.01	0	–0.01	0.01
ZIR	27.54	93.8	–2.43	–2.14	–0.3	–3.84	–3.71	–0.14
					0.04			0.05

which gives a ratio of 951. Although the ratio of the largest singular value to the smallest one less than 200 is adequate to assure reliable solutions, larger ratios do not necessarily translate into numerical problems[12]. In this context, an important check is the sum of the station corrections, which should be equal to the sum of their initial estimates, and is routinely assigned to a value of zero. In our study, the sum of station corrections is equal to -3.18×10^{-4}, close to the expected value of zero.

The JHD station corrections provide valuable information about velocity variations[27]. By forward modelling of the station corrections it is possible to infer the gross features of the velocity structure[30]. The *P*-wave station correction ranges between –2.43 and 2.32 s, and the *S*-wave station correction between –2.84 and 2.84 s. The wide range of corrections indicates the presence of lateral variations of velocity in the study area. Pujol[12] and Ratchkovsky *et al.*[27] have reported that positive station corrections are associated with low velocity features at shallower depth, such as basin areas underlain by alluvium, and the negative corrections with higher velocity features and hills. In this study, the positive *P*-wave station-correction contours correspond to the Shillong Plateau, upper Assam valley and the Manipur Fold Belt areas, and negative contours correspond to the Mikir hills and the Kopili lineament (Figure 5 *a*). Similar results are indicated by the *S*-wave station corrections (Figure 5 *b*). The observed and synthetic JHD corrections are also in good agreement (Table 3). We believe that the results obtained by the JHD method represent the lateral velocity variations and not artifacts. This is further compared with the shallow (depth 5 km) velocity structure obtained by the LET method (Figure 5 *c*). It is observed that the low velocity seismic structures are comparable with the positive *P*-wave station correction contours in the Shillong Plateau, upper Assam valley and the Manipur Fold Belt areas, and the high seismic velocity with the negative *P*-wave station correction contours in the Mikir hills. Thus the analysis of synthetic data as well as the 3D velocity structure obtained by LET gives further confidence to the JHD locations.

The positive station corrections in the Shillong Plateau, upper Assam valley and Manipur Fold Belt may be explained by the tectonic/geologic setting of the region. The Shillong Plateau is conspicuous with high gravity anomaly[31], indicating the presence of antiroot or nearness of mantle material implying shallow crustal thickness. Low velocity seismic structure has been reported for the upper crust (~ 5 km) beneath the Shillong Plateau[5]. Gupta and Singh[31] observed a positive *P*-wave residual anomaly of about 0.4 s in the Shillong plateau and reported that the *P*-wave velocity of the crust in the plateau decreased since 1970, and the same trend continues. They suggested that the region is experiencing a dilatancy stage, which is a precursor to large earthquakes. The upper Assam valley, covered with thick (~ 3 km) alluvium sediments, shows positive station correction, indicating low velocity sediments. The Manipur Fold Belt comprises of the Cretaceous–Tertiary flysch sediments, is also manifested by low gravity anomaly[32], and the upper crust with a low *P*-wave velocity indicates positive station correction.

The negative station corrections in the Mikir hills and along the Kopili lineament are interesting. The higher crustal velocity structures obtained by LET below the Mikir hills and that below the Kopili lineament (Figure 5 *c*) are well reflected by negative station corrections (Figure 5 *a*). There is a broad agreement between the negative station

correction and the higher crustal velocity, as well as the positive station correction and the low velocity crust in the region.

We have plotted *S*-wave versus *P*-wave station corrections for both actual and synthetic data (Figure 6). In both the cases, the *S*-wave station correction closely follows the *P*-wave correction. In Figure 6 *b*, one observation (at station CDL situated in the Manipur Fold Belt) shows a deviation. This station may not have properly recorded the *S*-wave. This synthetic test shows that the JHD method is also capable of identifying errors in phase identification.

The JHD technique has not only improved the hypocentre locations, the estimated station corrections qualitatively reflect the lateral velocity variations at shallow depth. The station corrections are comparable with the geologic and tectonic features as well as with the estimated 3D velocity structures. The JHD is an inexpensive and semi-qualitative method for 3D velocity assessment at shallow depth. Since the relative locations are more precise in this method true seismicity patterns are well reflected, particularly in the depth section.

1. Khattri, K. N., Wyss, M., Gaur, V. K., Saha, S. K. and Bansal, V. K., Local seismic activity in the region of the Assam gap, northeast India. *Bull. Seismol. Soc. Am.*, 1983, **73**, 459–469.
2. Kayal, J. R., Microseismicity and source mechanism study: Shillong Plateau, Northeast India. *Bull. Seismol. Soc. Am.*, 1987, **77**, 184–194.
3. Kayal, J. R. and De, R., Microseismicity and tectonics in northeast India. *Bull. Seismol. Soc. Am.*, 1991, **81**, 131–138.
4. Kayal, J. R., Earthquake source processes in northeast India: A review. *J. Himalayan Geol.*, 1996, **17**, 53–69.
5. Kayal, J. R. and Zhao, D., Three dimensional seismic structure beneath Shillong plateau and Assam valley, northeast India. *Bull. Seismol. Soc. Am.*, 1998, **88**, 667–676.
6. Bhattacharya, P. M., Majumdar, R. K. and Kayal, J. R., Fractal dimension and b-value mapping in northeast India. *Curr. Sci.* 2002, **82**, 1486–1491.
7. Engdahl, E. R., Dewey, J. W. and Fujita, K., Earthquake location in island arcs. *Phys. Earth Planet. Inter.*, 1982, **30**, 145–156.
8. Pujol, J., Comments on the joint determination of hypocenters and station corrections. *Bull. Seismol. Soc. Am.*, 1988, **78**, 1179–1189.
9. Pujol, J., An integrated 3D velocity inversion – Joint Hypocentral Determination relocation analysis of events in the Northridge area. *Bull. Seismol. Soc. Am.*, 1996, **86**, S138–S155.
10. Lahr, J. C., HYPOELLIPSE: A computer program for determining local earthquake hypocentral parameters, magnitude, and first motion pattern. US Geol. Surv. Open-File Rep. 79–431, 1979.
11. Lee, W. H. K. and Valdes, C. M., *User Manual for HYPO71PC*, *IASPEI Software Library*, 1989, vol. 1, pp. 203–236.
12. Pujol, J., Application of the JHD technique to the Loma Prieta, California, mainshock-aftershock sequence and implications for earthquake location. *Bull. Seismol. Soc. Am.*, 1995, **80**, 129–150.
13. Thurber, C. H., Earthquake locations and three-dimensional crustal structure in the Coyote Lake area, central California. *J. Geophys. Res.*, 1983, **88**, 8226–8236.
14. Seeber, L., Armbuster, J. G. and Quittmeyer, R., Seismicity and continental subduction in the Himalayan Arc. *Geodyn. Ser.* 1981, **3**, 215–242.
15. Kayal, J. R., De, R. and Chakraborty, P., Microearthquakes at the Main Boundary Thrust in eastern Himalaya and the present day tectonic model. *Tectonophysics*, 1993, **218**, 375–381.
16. Ni, J. and Barazangi, M., Seismotectonics of the Himalayan collision zone: Geometry of the underthrusting Indian plate beneath the Himalaya. *J. Geophys. Res.*, 1984, **89**, 1147–1163.
17. Kayal, J. R., Microearthquake activity in some parts of the Himalaya and the tectonic model. *Tectonophysics*, 2001, **339**, 331–351.
18. Mukhopadhyay, M. and Dasgupta, S., Deep structure and tectonics of the Burmese Arc: Constraints from earthquake and gravity data. *Tectonophysics*, 1988, **149**, 299–322.
19. Kumar, M. R. and Rao, N. P., Significant trends related to slab seismicity and tectonics in the Burmese Arc region from Havard CMT solutions. *Phys. Earth Planet. Inter.*, 1995, **90**, 75–80.
20. Biswas, S. and and Majumdar, R. K., Seismicity and tectonics of the Bay of Bengal : Evidence for intraplate deformation of the northern Indian plate. *Tectonophysics*, 1997, **269**, 323–336.
21. Nandy, D. R., *Geodynamics of Northeastern India and the Adjoining Region*, acb Publication, Calcutta, 2001.
22. Wadati, K., On the travel times of earthquake waves, Part II. *Geophys. Mag.*, 1933, **7**, 101–111.
23. Lee, W. H. K. and Lahr, J. C., A computer program for determining hypocenter, magnitude and first motion pattern of local earthquakes. *HYPO71* (revised): US Geol. Surv. Open-File Rep., 1975, vol. 75–311, pp. 1–116.
24. De, R. and Kayal, J. R., Crustal P-wave velocity and velocity-ratio study in northeast India by a microearthquake survey. *Pure Appl. Geophys.*, 1990, **134**, 93–108.
25. Eberhart Phillips, D., Local earthquake tomography: earthquake source regions. In *Seismic Tomography: Theory and Practice* (eds Iyer, H. M. and Hirahara, K.), Chapman and Hall, London, 1993, pp. 613–643.
26. Pavilis, G. and Booker, J., Progressive multiple event location (PMEL). *Bull. Seismol. Soc. Am.*, 1983, **73**, 1753–1777.
27. Ratchkovsky, N. A., Pujol, J. and Biswas, N. N., Relocation of earthquakes in the Cook Inlet area, South Central Alaska, Using the joint hypocenter determination method. *Bull. Seismol. Soc. Am.*, 1997, **87**, 620–636.
28. Bhattacharya, P. M., Mukhopadhyay, S., Majumdar, R. K. and Kayal, J. R., 3-D Seismic structure of the Northeast India region and its implications for local and regional tectonics. *Geophys. J. Int.*, 2005, submitted.
29. Pujol, J., Earthquake location tutorial: Graphical approach and approximate epicentral location techniques. *Seismol. Res. Lett.*, 2004, **75**, 63–74.
30. Pujol, J., Comments on the joint determination of hypocenters and station corrections. *Bull. Seismol. Soc. Am.*, 1992, **78**, 1179–1189.
31. Gupta, H. K. and Singh, V. P., Teleseismic P-wave residual investigations at Shillong, India.*Tectonophysics*, 1980, **66**, 19–27.
32. Verma, R. K. and Mukhopadhyay, M., An analysis of the gravity field in northeastern India. *Tectonophysics*, 1977, **42**, 283–317.
33. Kayal, J. R., Seismicity of northeast India and surroundings – development over the past 100 years. *J. Geophys.*, 1998, **XIX**, 9–34.

ACKNOWLEDGEMENTS. We thank the Director General, GSI, Kolkata for approval of the research project. We thank the Head, Geoscience Division, RRL(J), for providing seismological bulletins.

Received 20 January 2005; revised accepted 23 June 2005